Supplementary information:

Sample preparation

$LiFe_{1-x}Co_xAs$ single crystals were grown with self-flux method. The basic sample characterization was described in the previous papers [1-3]. Samples used in this report were grown with isotope ^7Li to reduce the neutron absorption and wrapped by Aluminum foil with Hydrogen-free glue to avoid exposure to air and humidity. The sample growth work was carried out at Beijing National Laboratory for Condensed Matter Physics, Institute of Physics, Chinese Academy of Science and at Rice University.

Background subtraction and data analysis

In a typical time-of-flight experiment, the raw inelastic neutron scattering data at certain energy are shown in Fig. S1(a). In order to obtain the background, we masked the signal area, for instance, the white square in Fig. S1(b). Assuming the background in our time-of-flight data is radially symmetric, we integrated the remaining intensity and fitted it with a polynomial function of |Q| to the second order as shown in Fig. S1(c). Then we used this fitted polynomial function as background and subtracted it from the raw neutron scattering data. The final subtracted data was shown in Fig. S1(d) and Fig. S1(e).

In Fig. S2, we show a series of typical subtracted constant-energy cuts from 10 meV to 220 meV. These cuts were fitted with one or two Gaussian functions. We show the fitted result in previous Fig. 4(a). It is worth noting that the x-errors in Fig. 4(a) are the fitted peak width.

RPA calculation

In Fig. S3, we demonstrate the existence of two transversely incommensurate peaks in the dynamic spin susceptibility with differentiated orbital character for LiFeAs. Electron-doping in $LiFe_{0.88}Co_{0.12}As$ is introduced by rigid band shift. The starting point for our calculation is an effective 10-orbital tight-binding Hamiltonian derived from ARPES and symmetry considerations [4] and previously discussed in Ref. [5]. We calculate the noninteracting bare susceptibility along high-symmetry cuts, considering lowest-order scattering processes as described previously [5] [6]:

$$\chi^0_{l_1 l_2 l_3 l_4}(\mathbf{q},\omega) = -\frac{1}{N}\sum_{\mathbf{k},\mu\upsilon}\frac{a^{l_4}_{\mu}(\mathbf{k})a^{l_2,*}_{\mu}(\mathbf{k})a^{l_1}_{\upsilon}(\mathbf{k}+\mathbf{q})a^{l_3,*}_{\upsilon}(\mathbf{k}+\mathbf{q})}{\omega + E_{\mu}(\mathbf{k}) - E_{\upsilon}(\mathbf{k}+\mathbf{q}) + i\delta}\Big(f\left[E_{\mu}(\mathbf{k}),kT\right] - f\left[E_{\upsilon}(\mathbf{k}+\mathbf{q}),kT\right]\Big), \quad (1)$$

with $N = 2$ the number of iron sites per unit cell, band indices μ and υ, orbital indices l. The matrix elements are represented by the orbital projection of the Bloch state, $a_\mu^l = \langle l \,|\, \mu \mathbf{k} \rangle$ and $f\left[E, kT\right]$ is the Fermi function at temperature T. We use $T = 100K$, a small parameter $\delta = 0.005$ to enforce analyticity, and sum over a k-space mesh of $120 \times 120 \times 8$ points over the 3D Brillouin zone, which we find to be sufficiently dense to accurately describe the susceptibility everywhere in reciprocal space.

RPA interactions are applied in a manifestly spin-rotationally invariant form, using the intra-orbital Coulomb repulsion $U = 0.6$ eV and Hund's coupling $J = 0.15$, and inter-orbital Coulomb interaction $U' = 0.3$ and pair-hopping $J' = 0.15$, with the same interaction strengths applied identically over all ten d-orbitals. These values for the interactions are just below their maximum values, as determined when the susceptibility diverges at the antiferromagnetic wave vector Q in the doped compound. Because the intra-orbital scattering is dominant in the total RPA susceptibility, we focus on intra-orbital components of the bare susceptibility in the low energy limit, $\chi^0\left(\mathbf{q}, \omega = 10 \text{ meV}\right)$. To enable direct comparison to neutron scattering, where the orthorhombic structure factor forbids scattering at even L, we fix $q_z = \pi / c$ (L=1).

We find the scattering peaks in the parent compound ($\langle n \rangle = 12.00$) at $\Delta\mathbf{Q} \approx 0.18$ and 0.3, quite consistent with the incommensurabilities suggested by Fermi surface nesting shown in Fig. 1(c)-(d). After the application of RPA interactions, tracing only over the d_{xy} (d_{xz}) orbitals selectively amplifies the narrower (wider) peaks; in other words, considering the system with and without interactions, the results are qualitatively identical. In the electron-doped case ($\langle n \rangle = 12.24$), the single obvious feature is the commensurate peak, which has predominantly d_{xy} character.

DFT+DMFT calculation

Density functional theory (DFT) calculations were done using the full-potential linear augmented plane wave method implemented in Wien2K[7] in conjunction with a generalized gradient approximation[8] of the exchange correlation functional. To take into account strong correlation effect, we further carried out first-principles calculations using a combination of density functional theory and dynamical mean field theory (DFT+DMFT)[9] which was implemented on top of Wien2K and documented in Ref. [10]. In the DFT+DMFT calculations, the electronic charge was computed self-consistently on DFT+DMFT density matrix. The quantum impurity problem was solved by the continuous time quantum Monte Carlo (CTQMC) method[11,12], using Slater form of the Coulomb repulsion in its fully rotational invariant form. Consistent with previous publication[13,14], we used a Hubbard U=5.0 eV and Hund's rule coupling J=0.8 eV, and

experimentally determined crystal structure for LiFeAs[15], including the internal positions of the atoms. The Co-doping is simulated using virtual crystal approximation (VCA) in the DFT+DMFT calculation. The bare susceptibility was computed using the fully self-consistent DFT+DMFT lattice Green's function and the spin susceptibility was computed using the Bethe-Salpeter equation which takes into account two-particle vertex correction. Here the two-particle (particle-hole) irreducible vertex is local within DMFT and it is equal to the impurity vertex, which can be obtained from the solution of the quantum impurity model using CTQMC. Further computational details on spin susceptibility are available in Ref.[14].

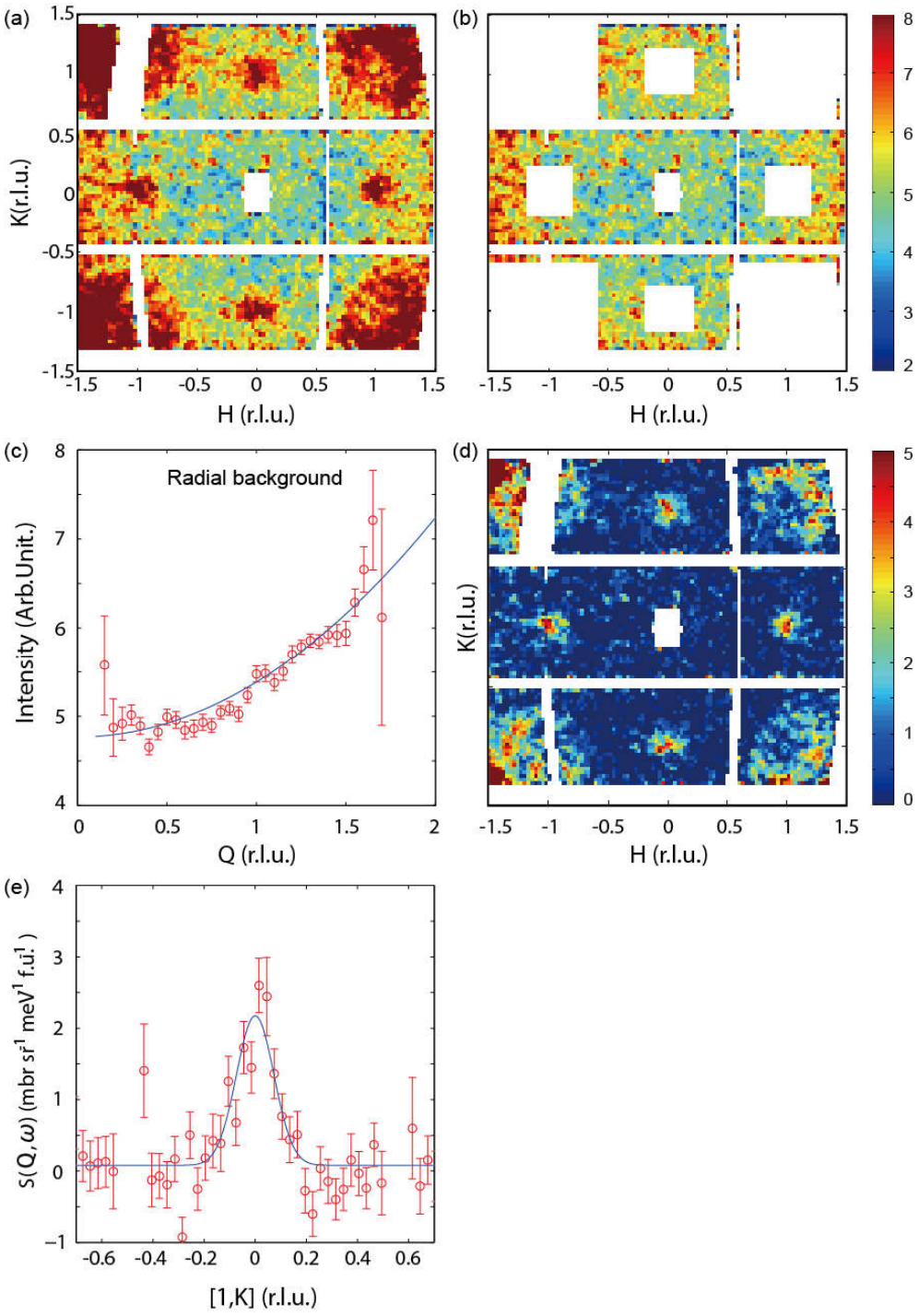

Figure S1. (Color online) (a).Constant energy map of the raw data at E=[6,8] meV in $LiFe_{0.88}Co_{0.12}As$. (b) The background intensity in which all the phonon and magnon signals are masked. (c) We get the radially symmetric background from (b) and fit it with a parabolic function. (d) The constant energy map after background subtraction. (e) A cut along [1,H] direction in panel (d).

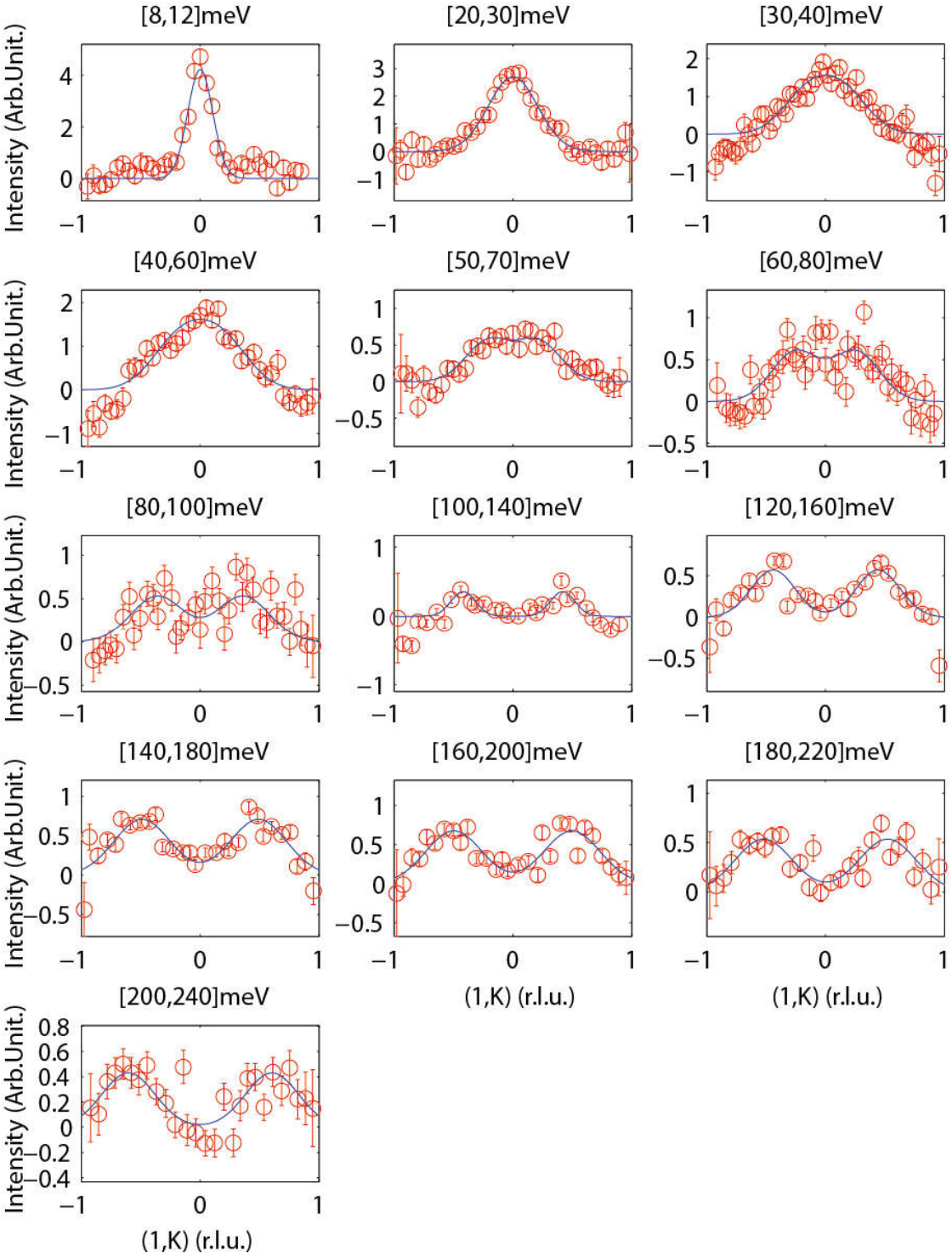

Figure S2. (Color online) Energy dependence of the 1-d cut of the spin excitations along [1, K] direction in $LiFe_{0.88}Co_{0.12}As$. The peaks are fitted with Gaussian functions and the fitted results are shown in Fig. 4(a). The energy ranges shown here are the E-errors and the peak widths are q-errors Fig. 4(a).

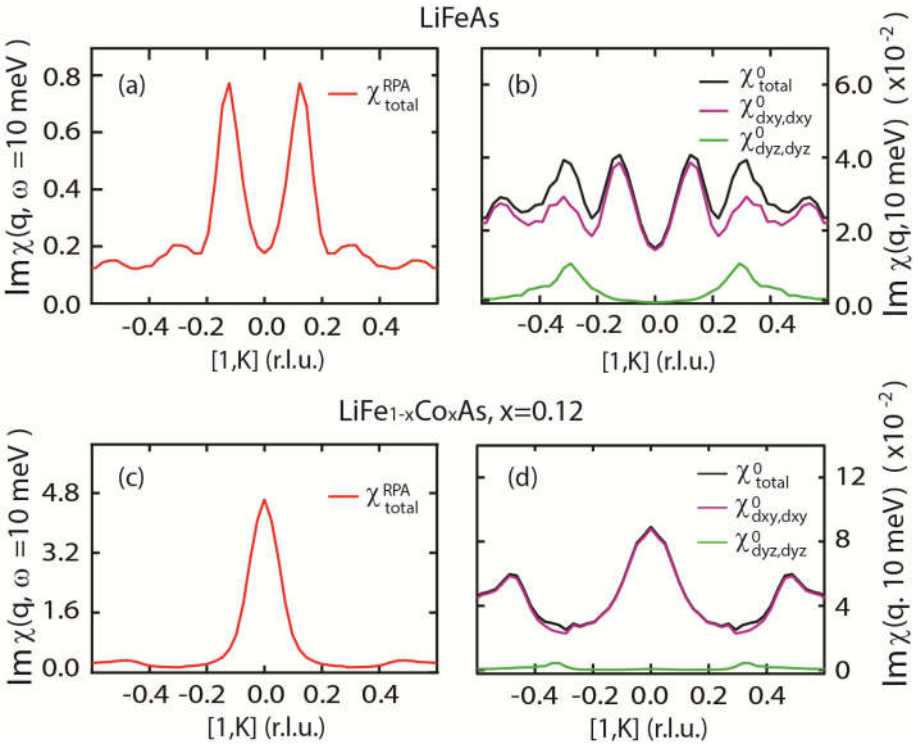

Figure S3. (Color online) LDA+RPA calculation of dynamic spin susceptibility in LiFeAs and $LiFe_{0.88}Co_{0.12}As$. (a),(c) Wave vector dependence of the imaginary part of total RPA susceptibility at 10 meV for LiFeAs and $LiFe_{0.88}Co_{0.12}As$. Note that the peak position changes from incommensurate wave vector in LiFeAs to commensurate in 12% electron doped compound, consistent with the our experimental result (Fig.1 (b)). (b),(d) The calculated bare susceptibility of LiFeAs and $LiFe_{0.88}Co_{0.12}As$. The black curve represents the total bare susceptibility while the purple (green) one shows the intra-orbital component of d_{xy} (d_{yz}) orbital. Note that the main peaks observed in LiFeAs mainly come from $\chi_{xy,xy}$ scattering channel while the $\chi_{yz,yz}$ (or $\chi_{xz,xz}$ due to the existence of four-fold symmetry) component almost vanishes when T_c is suppressed in $LiFe_{0.88}Co_{0.12}As$.

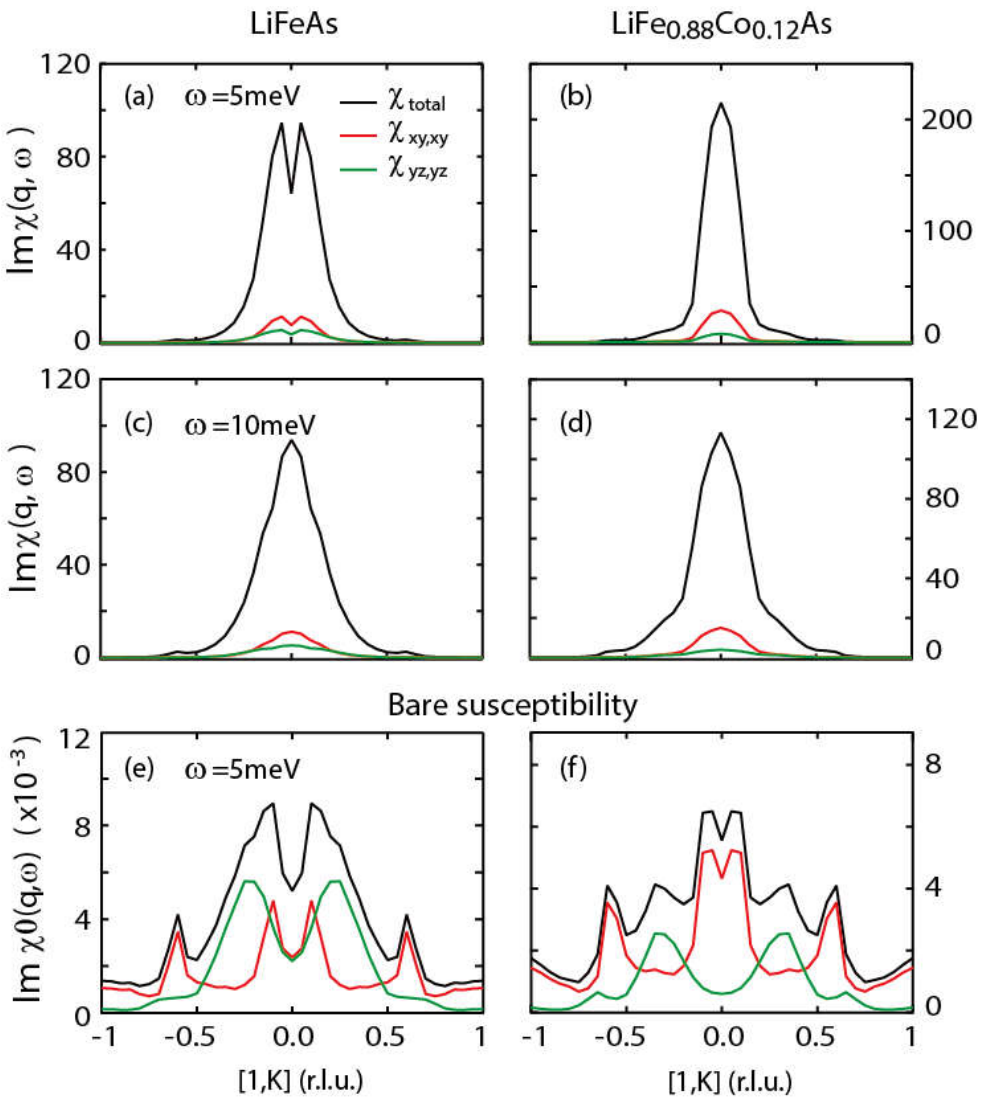

Figure S4. (Color online) The dynamic spin susceptibility from DFT+DMFT calculation for LiFeAs and $LiFe_{0.88}Co_{0.12}As$. (a),(b) The imaginary part of spin susceptibility at 5 meV for LiFeAs and $LiFe_{0.88}Co_{0.12}As$, respectively. The black curves represent the total susceptibility and the red (green) ones are the $\chi_{xy,xy}$ ($\chi_{yz,yz}$) components. (c),(d) The corresponding total and orbital components of spin susceptibility at 10 meV for LiFeAs and $LiFe_{0.88}Co_{0.12}As$. (e), (f) are bare susceptibility for LiFeAs and $LiFe_{0.88}Co_{0.12}As$, respectively, at 5 meV. The doping dependence of the incommensurability is similar to the experimental result and LDA+RPA calculation. Note that in 12% Co doped compound, the $\chi_{xy,xy}$ component is actually enhanced while $\chi_{yz,yz}$ component is suppressed. The overall intensity of total susceptibility within this energy range is also enhanced a little bit, in sharp contrast to great suppression the superconducting temperature (T_c) in this compound.

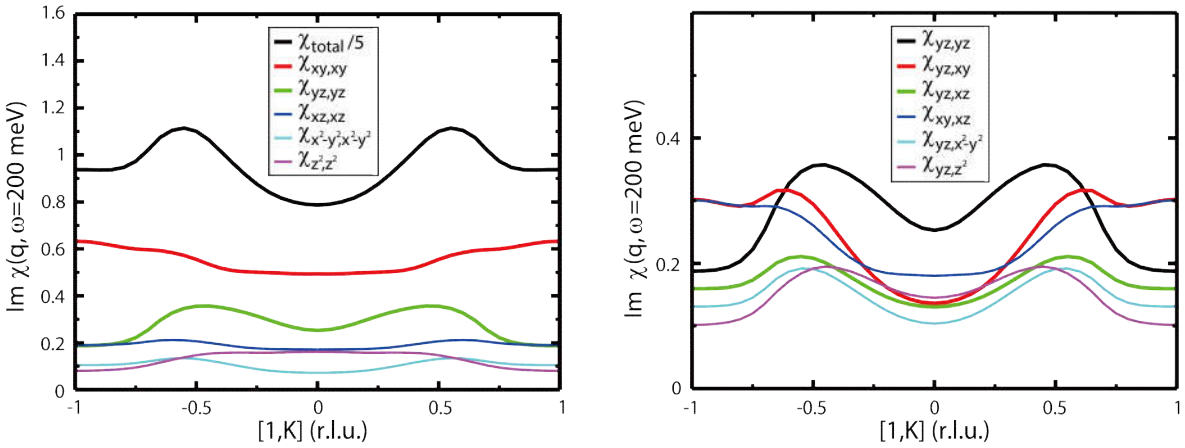

Figure S5. (Color online) (a) The intra-orbital components of dynamic susceptibility at 200 meV (mainly upper branch) for $LiFe_{0.88}Co_{0.12}As$. It is clearly seen that the peaks in the total susceptibility mainly come from $\chi_{yz,yz}$ intra-orbital part. (b) Comparison between intra-orbital and inter-oribtal components which are associated with d_{yz} orbital. The intra-orbital $\chi_{yz,yz}$ component is apparently dominant while the inter-orbital channels contribute a small part in the total spin susceptibility at 200 meV.

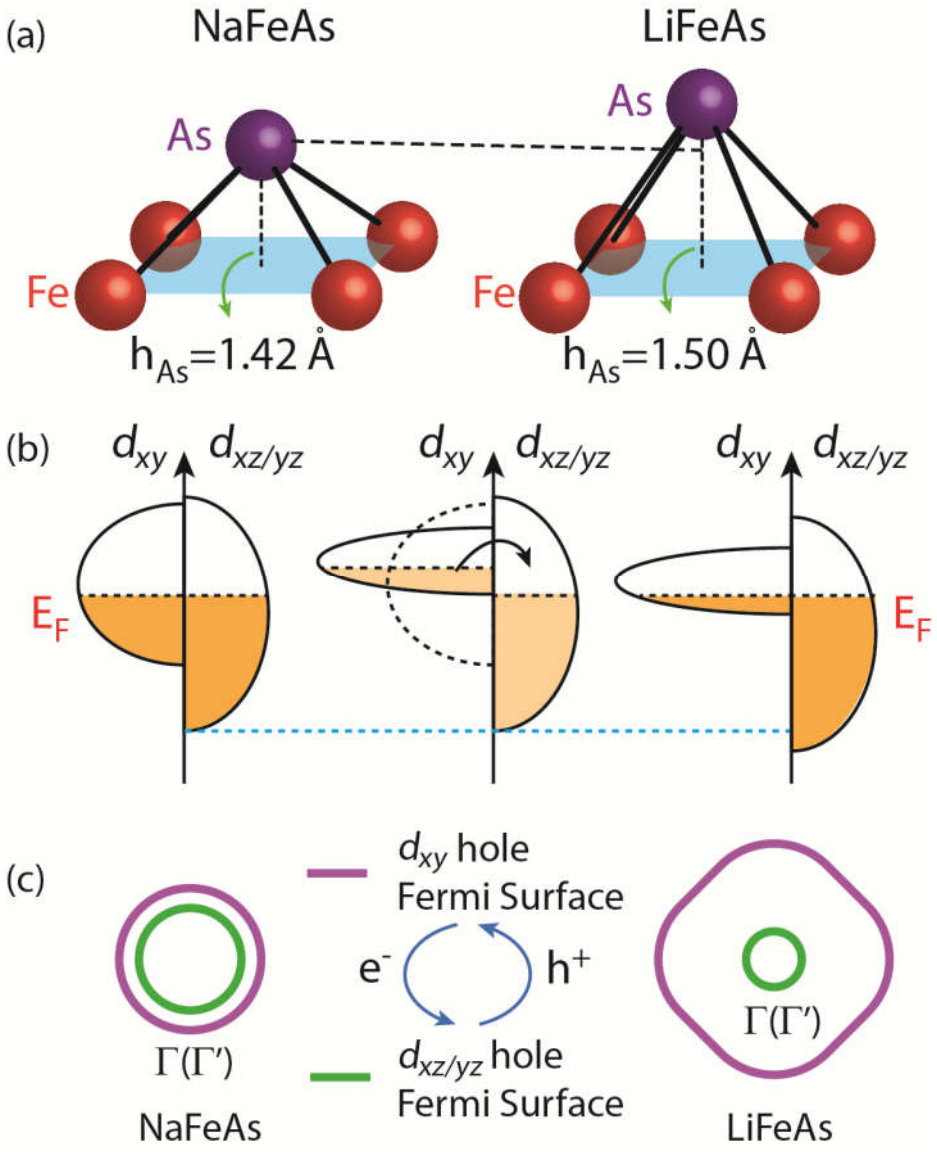

Figure S6. (Color online) (a) The structure of the Fe-As layer in NaFeAs and LiFeAs. The anion height in LiFeAs ~ 1.5 Å (Ref. [2]) is larger than that in NaFeAs ~1.42 Å (Ref. [3]). (b) Illustration of the orbital dependent band renormalization and subsequent charge transfer from d_{xy} to $d_{xz/yz}$ orbitals. The renormalization is overstated to emphasize the orbital dependent effect. The situation in reality might be even more complicated due to the strong hybridization with As p orbitals [6]. (c) Comparison of the Fermi Surface in NaFeAs and LiFeAs. The orbital dependent band renormalization (panel (b)) drives electrons (holes) from d_{xy} ($d_{xz/yz}$) to $d_{xz/yz}$ (d_{xy}), resulting in an enlarged outer d_{xy} hole FS and a reduced inner $d_{xz/yz}$ pockets in LiFeAs.

Reference

[1] L.Y. Xing, H Miao, X.C. Wang, J Ma, Q.Q. Liu, Z. Deng, H. Ding and C.Q. Jin, *J.Phys.: Condens. Matter* **26**, 435703 (2014)

[2] Michael J. Pitcher, Dinah R. Parker, Paul Adamson, Sebastian J.C. Herkelrath, Andrew T. Boothroyd, Richard M. Ibberson, Michela Brunelli and Simon J. Clarke , *Chem. Commun.*, 2008, 5918–5920

[3] D. R. Parker, M. J. Pitcher, P. J. Baker, I. Franke, T. Lancaster, S. J. Blundell, and S. J. Clarke, *Chem. Commun.*, 2009, 2189–2191

[4] H. Eschrig and K. Koepernik, *Phys. Rev. B* **80**, 104503 (2009).

[5] Y. Wang, A. Kreisel, V. Zabolotnyy, S. Borisenko, B. Bchner, T. Maier, P. Hirschfeld, and D. Scalapino, *Phys. Rev. B* **88**, 174516 (2013).

[6] K. Kuroki, S. Onari, R. Arita, H. Usui, Y. Tanaka, H. Kontani, and H. Aoki, *Phys. Rev. Lett.* **101**, 087004 (2008).

[7] P. Blaha, K. Schwarz, G. K. H. Madsen, D. Kvasnicka and J. Luitz, **WIEN2K** (K. Schwarz, Techn. Univ. Wien, Austria, 2001).

[8] J. P. Perdew, K. Burke, and M. Ernzerhof, *Phys. Rev. Lett.* **77**, 3865-3868 (1996).

[9] G. Kotliar, S. Y. Savrasov, K. Haule, V. S. Oudovenko, O. Parcollet, and C. A. Marianetti, *Rev. Mod. Phys.* **78**, 856 (2006).

[10] K. Haule, C.-H. Yee, K. Kim, *Phys. Rev. B* **81**, 195107 (2010).

[11] Kristjan Haule, *Phys. Rev. B* **75**, 155113 (2007).

[12] P. Werner, A. Comanac, L. de Medici, M. Troyer, and A. J. Millis, *Phys. Rev. Lett.* **97**, 076405 (2006).

[13] Z. P. Yin, K. Haule, and G. Kotliar, *Nat. Mater.* **10**, 932 (2011).

[14] Z. P. Yin, K. Haule, G. Kotliar, *Nat. Phys.* **10**, 845 (2014).

[15] J. H. Tapp, Zhongjia Tang, Bing Lv, Kalyan Sasmal, Bernd Lorenz, Paul C.W. Chu, and Arnold M. Guloy, *Phys. Rev. B* **78**, 060505(R) (2008).